

Review of key vertical-cavity laser and modulator advances enabled by advanced MBE technology

Cite as: J. Vac. Sci. Technol. A **39**, 010801 (2021); <https://doi.org/10.1116/6.0000574>

Submitted: 23 August 2020 . Accepted: 04 November 2020 . Published Online: 30 November 2020

Larry A. Coldren

COLLECTIONS

Paper published as part of the special topic on [Honoring Dr. Art Gossard's 85th Birthday and His Leadership in the Science and Technology of Molecular Beam Epitaxy ART2020](#)



View Online



Export Citation



CrossMark

ARTICLES YOU MAY BE INTERESTED IN

[Universal scaling relationship for atomic layer etching](#)

Journal of Vacuum Science & Technology A **39**, 010401 (2021); <https://doi.org/10.1116/6.0000762>

[Practical guide to the use of backgrounds in quantitative XPS](#)

Journal of Vacuum Science & Technology A **39**, 011201 (2021); <https://doi.org/10.1116/6.0000661>

[Introduction to x-ray photoelectron spectroscopy](#)

Journal of Vacuum Science & Technology A **38**, 063204 (2020); <https://doi.org/10.1116/6.0000412>



HIDEN
ANALYTICAL

Instruments for Advanced Science

Contact Hiden Analytical for further details:
www.HidenAnalytical.com
info@hiden.co.uk

[CLICK TO VIEW](#) our product catalogue



Gas Analysis

- dynamic measurement of reaction gas streams
- catalysis and thermal analysis
- molecular beam studies
- dissolved species probes
- fermentation, environmental and ecological studies



Surface Science

- UHV/TPD
- SIMS
- end point detection in ion beam etch
- elemental imaging - surface mapping



Plasma Diagnostics

- plasma source characterization
- etch and deposition process reaction kinetic studies
- analysis of neutral and radical species



Vacuum Analysis

- partial pressure measurement and control of process gases
- reactive sputter process control
- vacuum diagnostics
- vacuum coating process monitoring



Review of key vertical-cavity laser and modulator advances enabled by advanced MBE technology

Cite as: J. Vac. Sci. Technol. A 39, 010801 (2021); doi: 10.1116/6.0000574
Submitted: 23 August 2020 · Accepted: 4 November 2020 ·
Published Online: 30 November 2020



Larry A. Coldren^{a)}

AFFILIATIONS

Electrical and Computer Engineering and Materials Departments, University of California, Santa Barbara, California 93106

Note: This paper is part of the Special Topic Collection: Honoring Dr. Art Gossard's 85th Birthday and his Leadership in the Science and Technology of Molecular Beam Epitaxy.

^{a)}Electronic mail: coldren@ucsb.edu

ABSTRACT

In this special issue honoring Professor Arthur Gossard, I am delighted to be able to review a small segment of the work he has enabled while at UCSB on the subject of the title, but further limited to devices grown all-epitaxially. When he arrived in 1987 from Bell Labs, he had already been consulting on the installation of our new Gen-II MBE that we intended to use for vertical-cavity Fabry–Pérot modulators, devices somewhat similar to those he had grown at Bell Labs. However, within a couple of years, we obtained leading results on reflection modulators, moving the on/off contrast from prior values of less than 5:1 to more than 50:1 with insertion losses of less than 2 dB, required voltages in the 2–4 V range, and changes in reflection per volt to $\sim 20\%/V$. These had multiple-quantum-well (MQW) active regions to phase shift and partially absorb the resonant lightwaves within a cavity formed between two distributed-Bragg-reflector (DBR) mirrors all formed in the AlGaAs/GaAs system. Also in this same period, novel vertical-cavity surface-emitting laser (VCSEL) structures analogous to the modulators were developed. They had strained InGaAs/GaAs MQW actives and AlGaAs/GaAs DBRs and operated near 980 nm. The initial new idea was to place active quantum wells only at the maxima of the cavity E-field standing wave, which provides nearly a doubling of the modal gain they contribute. These designs quickly led to leading results in threshold current ($<1 \text{ kA/cm}^2$ —1990 and $I_{\text{th}} < 1 \text{ mA}$ with $P_o > 1 \text{ mW}$ —1991), power out (up to 113 mW cw—1993), and temperature stability with gain offset (constant output over 50 °C—1993). Additional notable results in the 1990s included a selective oxidation of AlGaAs to form lens-like intra-cavity apertures for dramatic reductions in optical cavity loss; the first strained layer InGaAlAs/GaAs 850 nm VCSELs; and an 8-wavelength division multiplexing VCSEL array integrated within a 60 μm diameter for direct emission into a multimode fiber. In the 2000s, results included all-epitaxially grown 1310 nm and 1550 nm VCSELs that employed AlGaAsSb DBRs and AlGaInAs actives with tunnel junctions to enable two n-type contacts on InP for low thermal and electrical resistance; multi-terminal VCSELs for polarization modulation to double the information output on a single optical beam; and a novel high-speed, high-efficiency design that incorporated sophisticated bandgap engineering in the DBRs and carbon doping for low optical loss and electrical resistance, midlevel Al-content mirror layers near the cavity for deep oxidation to reduce capacitance, and a redesigned lens-like aperture for reduced mode volume. This latter design gave record modulation bandwidth and efficiency results then, and it is still being used around the world for the leading results today. In the most recent decade, InGaAsSb/AlGaAsSb/GaSb materials for VCSELs and photonic ICs have been studied for emission in the 2–4 μm wavelength range.

Published under license by AVS. <https://doi.org/10.1116/6.0000574>

I. INTRODUCTION

Professor Arthur Gossard has had, and continues to have, an extraordinary impact on semiconductor materials and device physics and technology, primarily through his work with molecular beam epitaxy (MBE). In this paper, I will review some highlights of the leading work he has enabled at UCSB on vertical-cavity optical modulators and lasers in which I have been involved. This represents a

relatively small component of his overall contributions over the past three-plus decades but, in my opinion, a component that has had a major impact on society. Some of his other contributions are mentioned in other articles in this issue.

Our first Varian Gen-II (system-A) had arrived shortly before Art in 1987 and was being used for AlGaAs and InGaAs/GaAs; the second one (system-B), which was interconnected to the first along

with a processing chamber via a transfer tube a couple of years later, had an Sb source for AlGaAsSb and eventually phosphorus capability for InP.

Our initial projects involved vertical-cavity reflection modulators,¹⁻⁷ so my students, now also guided by Art, worked on MBE system-A to grow multilayer stacks consisting of a bottom AlAs/Al_{0.2}Ga_{0.8}As multilayer DBR mirror, a GaAs/Al_{0.2}Ga_{0.8}As MQW active, and finally a top AlAs/Al_{0.2}Ga_{0.8}As multilayer DBR mirror. The number and thickness of layers in

each were varied for various designs. As will be detailed below, record-high on/off contrasts, with record-low drive voltages and insertion losses were developed within a few years. As codiscoverer of the quantum-confined Stark-effect (QCSE),⁸ a primary effect used in these devices, Art gave much more guidance than just on the MBE growth during this time.

In 1988, partially due to our modulator work, we came to the realization that a significant improvement could be made to the design of vertical-cavity surface-emitting-lasers (VCSELs) if the quantum-well gain layers were only placed at the cavity optical E-field standing wave maxima, and any losses were placed at the nulls.⁹⁻¹¹ In fact, this improvement changed the world of VCSEL design—for some number of quantum wells, the gain given to the optical mode would now be *doubled*, compared to a uniform placement of the wells along the standing wave. In practice, this meant

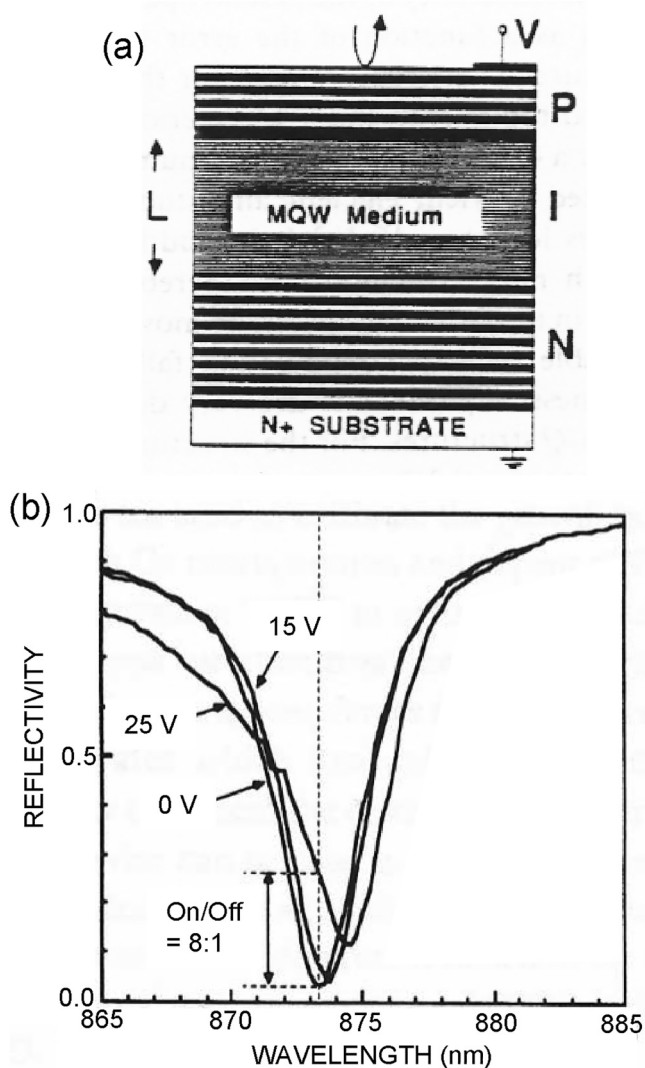


FIG. 1. (a) Schematic of MQW index modulator. Here, the top DBR mirror has five AlAs-Al_{0.2}Ga_{0.8}As periods, active MQW has 103–10 nm GaAs QWs with 10 nm Al_{0.2}Ga_{0.8}As barriers and the bottom DBR has 8.5 AlAs-Al_{0.2}Ga_{0.8}As periods. (b) Reflection spectra for reverse bias voltages of 0, 15, and 25 V. Adapted with permission from Simes *et al.*, Appl. Phys. Lett. **53**, 637 (1988). Copyright 1988, AIP Publishing LLC.

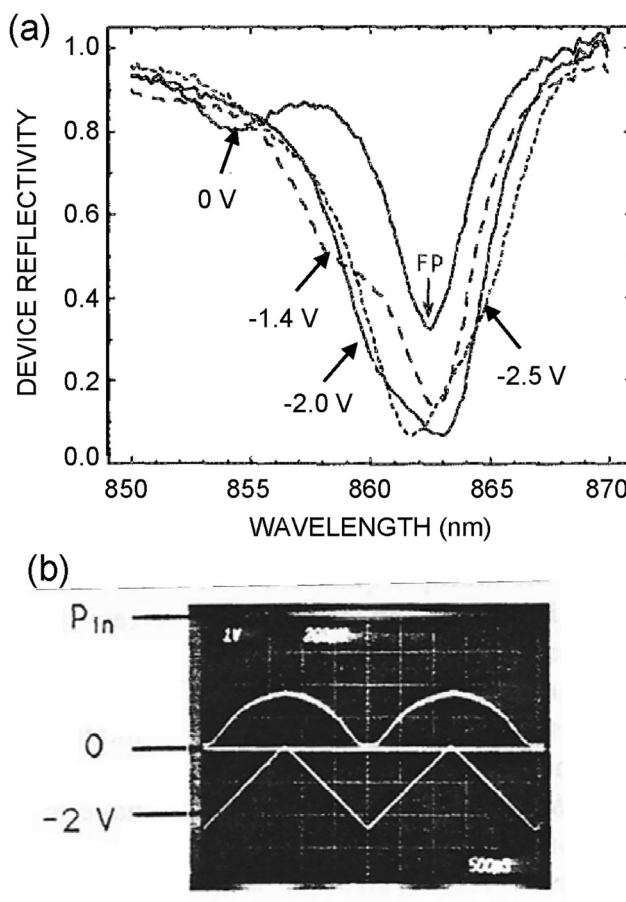


FIG. 2. (a) Reflection spectra with four reverse bias voltages from 0 to 2.5 V. (b) Sweeps of reflected power (top) and reverse bias (bottom) vs time; (500 μs/div.) Device schematic as in Fig. 1(a). Top and bottom mirror stacks had 5 and 20.5 periods of AlAs/Al_{0.2}Ga_{0.8}As, respectively; active MQW had 24 periods of 10 nm GaAs QWs with 10 nm Al_{0.2}Ga_{0.8}As barriers. Adapted with permission from Yan *et al.*, Appl. Phys. Lett. **56**, 1626 (1990). Copyright 1990, AIP Publishing LLC.

that the number of wells could be cut in half to reach threshold gain, the threshold current could be halved, the threshold power dissipation cut to a quarter, and most importantly, devices that could not work at all due to heating would now work well. Other researchers picked up on this invention, and the race was on to demonstrate the first practical VCSELs using it. Although we convincingly demonstrated the concept with optical pumping of VCSELs grown with active regions having either uniform gain or properly placed segmented gain regions of the same net length,¹² we lost the race to demonstrate low threshold electrically pumped lasers by a couple of months to a joint Bell Labs—Bellcore effort.¹³

However, our devices were more advanced because we had added probe pads and antireflecting (AR)-coatings, which provided more power out.¹⁴ So, with our advanced MBE and processing

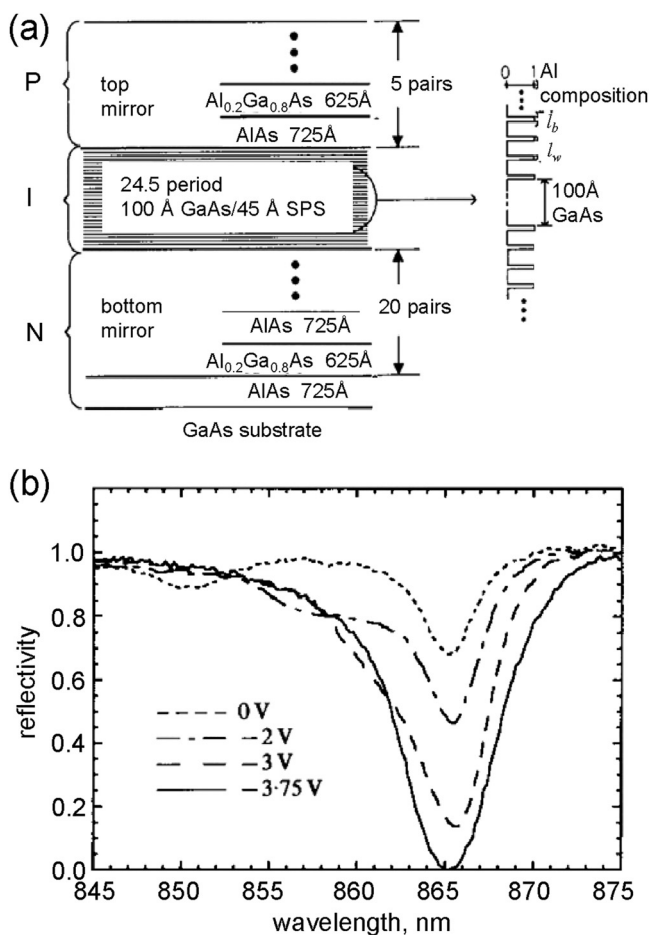


FIG. 3. (a) Schematic of an ASFP reflection modulator with short-period superlattice barriers in the 24.5 period active absorber region, which has 10 nm GaAs quantum wells and SPS barriers that are each a total thickness of 4.5 nm consisting of four $l_b = 0.34$ nm AlAs barrier layers spaced by three $l_w = 1.05$ nm GaAs well layers. The mirrors are similar to Fig. 2. (b) Reflection spectra of the ASFP modulator at the four labeled biases. Adapted with permission from Law *et al.*, *Electron. Lett.* **27**, 1863 (1991). Copyright 1991, IEE.

capability together with a team of outstanding graduate students, we were able to generate many of the leading results in low-threshold, high-output power, and temperature-stable VCSELs over the next couple of years.^{15–19} Additional innovations which followed included: strained-layer InGaAlAs/GaAs 850 nm VCSELs;²⁰ a lens-like intracavity aperture for a dramatic reduction in optical cavity loss;^{21,22} an 8-wavelength wavelength division multiplexing (WDM) VCSEL array;²³ all-epitaxially grown 1310 nm and 1550 nm VCSELs that employed AlGaAsSb DBRs and AlGaInAs actives on InP;^{24,25} multiterminal VCSELs for polarization modulation;^{26,27} and a novel high-speed, high-efficiency design that incorporated sophisticated bandgap engineering and carbon doping in the DBRs for low optical loss and electrical resistance, deep oxidation layers near the active to reduce capacitance, and a reduced mode volume.^{28–30} Results from all of the above will be reviewed below.

Most recently, InGaAsSb/AlGaAsSb/GaSb materials for VCSELs and photonic ICs have been studied for emission in the 2–4 μm wavelength range.³¹ These materials were grown in our Gen-III machine in collaboration with Prof. Palmström.

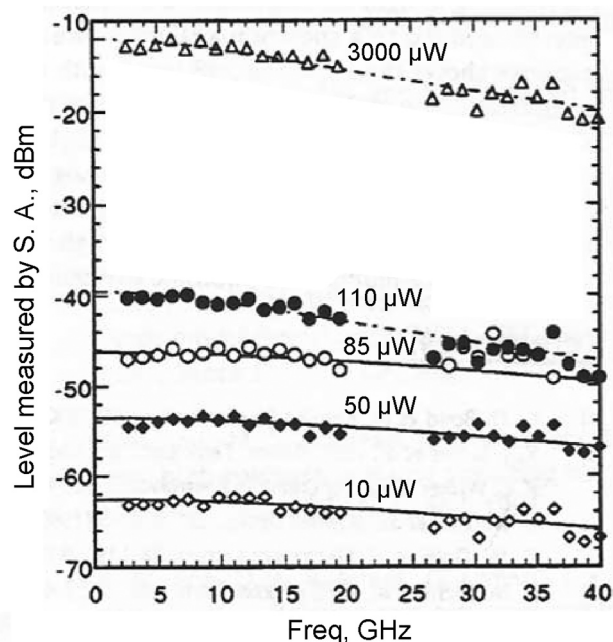


FIG. 4. High-speed, large-signal modulation from an ASFP with mm-wave contact pads, a semi-insulating substrate, a 2-period top mirror, and a 25-period bottom mirror, both containing quarter-wave AlAs/Al_{0.2}Ga_{0.8}As undoped DBR layers. The MQW active has 80 periods of 10 nm GaAs QWs and 4.5 nm Al_{0.3}Ga_{0.7}As barriers. Device lateral dimensions are $16 \times 20 \mu\text{m}$ and the cross section is as in Fig. 1(a) except for the addition of p and n contact layers immediately above and below the MQW active. Data are for increasing incident optical power levels as labeled. Theoretical RC-curve fits have 3 dB cut-offs at 37 GHz (solid) and 18 GHz (dashed). $\lambda = 864$ nm; bias = -12 V. Adapted with permission from *Device Research Conference*, Paper VIB-9, Santa Barbara, Jun. 23, 1993 (IEEE, Washington, DC, 1993); *ibid.* *IEEE LEOS'93*, Paper SP1.2, San Jose, Nov. 15, 1993 (IEEE, Washington, DC, 1993). Copyright 1993, IEEE.

In what follows, I will review the early vertical-cavity modulator results of the late 1980s and early 1990s that helped establish our MQW MBE program at UCSB. Then, I will continue with the early VCSEL work that grew out of the modulator work and required the need for good conduction through the DBR mirrors as well as good carrier injection into the QW active regions. The VCSEL discussion will then continue into the more recent efforts. Finally, I will conclude with what was learned and summarize its impact.

II. RESULTS ON MODULATORS

By the time Prof. Gossard arrived in 1987, my grad student, Rob Simes, had already grown early versions of a multiple-quantum-well

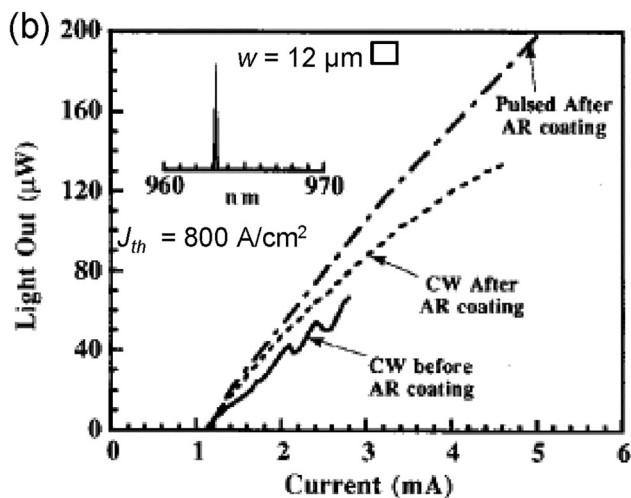
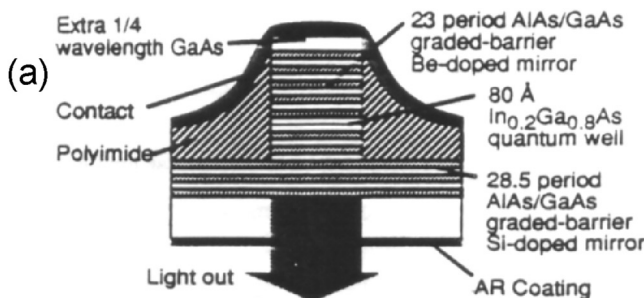


FIG. 5. Initial electrically pumped VCSEL results. (a) Schematic. Top p-doped mirror contained 23 AlAs-GaAs DBR periods; bottom n-doped mirror contained 28.5 AlAs-GaAs periods. Mirror interfaces were graded over 18 nm with digital superlattices. Doping was 4×10^{18} . Cavity had a single 8 nm $\text{In}_{0.2}\text{Ga}_{0.8}\text{As}$ QW surrounded by undoped 50 nm $\text{Al}_{0.5}\text{Ga}_{0.5}\text{As}$ layers on each side, and then this sandwich clad by p- or n-doped 80 nm $\text{Al}_{0.5}\text{Ga}_{0.5}\text{As}$ layers prior to the respective mirrors. (b) Light-out vs current-in results at 963 nm before and after AR-coating—CW, and pulsed after coating. Adapted with permission from Geels *et al.*, *Proceedings of Optical Fiber Communication Conference*, Paper PD31-1, San Francisco, Jan. 24, 1990 (OSA, Washington, DC, 1990). Copyright 1990, OSA.

(MQW) reflection modulator based on index modulation in our system A. This was accomplished in collaboration with Prof. Gossard and John English while they were still at Bell Labs. The results were submitted to the CLEO conference that Fall.³ Due to some imbalance, the device exhibited a 2:1 on/off contrast with 25 V of reverse bias and a minimum reflectivity of 15% at a wavelength of 882 nm, which at the time was still state-of-the-art.

With some improvements in the growth as well as moving the Fabry-Pérot resonance closer to the GaAs absorption edge (873 nm), where the QCSE is stronger, the result shown in Fig. 1 was obtained.⁴ In this case, the zero-bias reflection was only 3%, the contrast at 25 V was now 8:1, and there was also clear evidence of some absorption in addition to the index shift of the resonance with applied field.

The observation of the absorption effect led one of my students, R. H. Yan, to propose the primary use of absorption in addition to index in an asymmetric Fabry-Pérot (ASFP) reflection modulator design, which could require much lower drive voltage.^{5,6} The basic concept is to have a top mirror with modest reflection and a back mirror with a very high reflection, and then add loss to the cavity to make the back mirror “appear” to have a reflection like the front, and thus create a “balanced” cavity for zero reflection. To make it work all that was necessary was to modify the prior design by lengthening the back mirror and shifting the wavelength even closer to the absorption edge of the GaAs MQW. With a couple of iterations, it was found that fewer quantum-wells were needed in the active and thus, even lower voltages were obtainable. Figure 2 gives a result⁶ with only 24 quantum wells to lower the necessary drive voltage to 2 V, giving a reflection change of about 40% and an on/off contrast of >15.

Further refinements in the ASFPs included the exploration of novel superlattice active regions. One interesting example is illustrated in Fig. 3.⁷ Here, the AlGaAs barriers are replaced by relatively thin (4.5 nm) short-period superlattices (SPS) of AlAs/GaAs, and

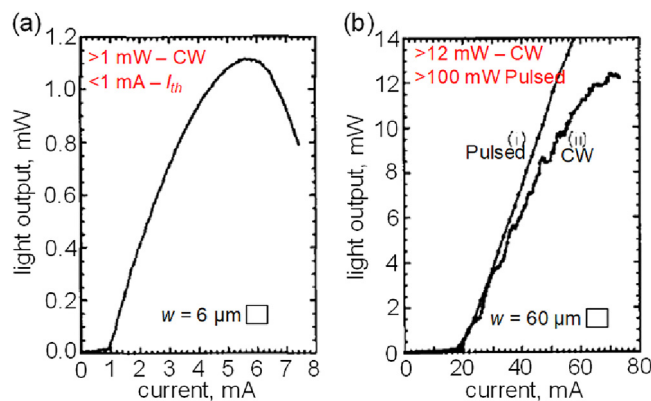


FIG. 6. VCSEL design similar to Fig. 5(a), except the number of periods in the top and bottom DBRs were 16 and 18.5, respectively, and the doping was reduced to 1×10^{18} , except in graded interfaces, where it increased to 5×10^{18} . Also, three 8 nm thick $\text{In}_{0.2}\text{Ga}_{0.8}\text{As}$ QWs were used. Parts (a) and (b) illustrate light-current results from two square mesa devices measuring either 6 or 60 μm on a side. $\lambda \sim 980$ nm. Adapted with permission from Geels and Coldren, *Electron. Lett.* 27, 1984 (1991). Copyright 1991, IEE.

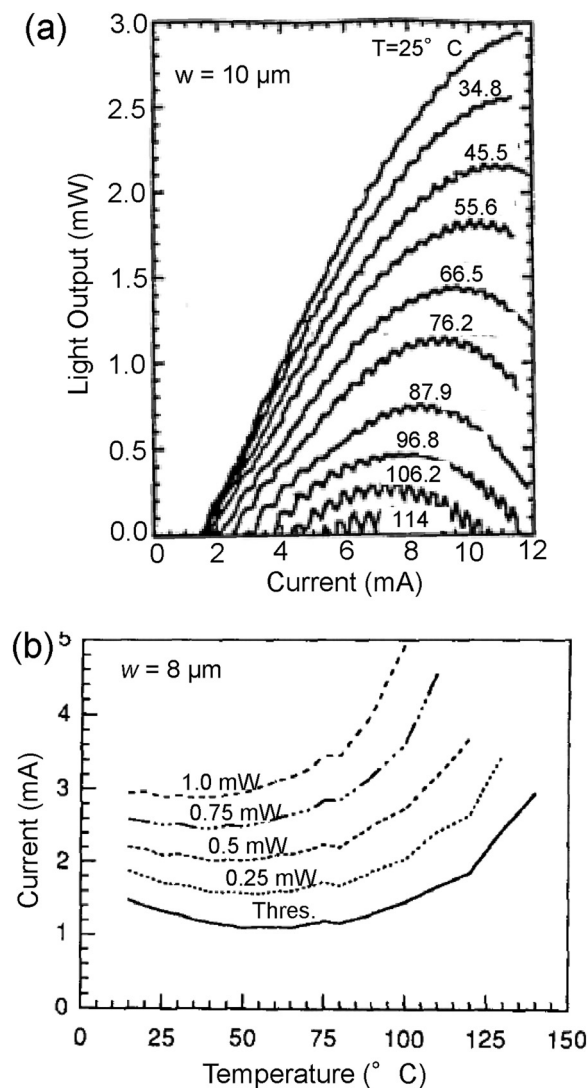


FIG. 7. Offset gain VCSELS. (a) Light-current characteristic for a VCSEL similar to a VCSEL described in Fig. 6, but with some gain offset introduced by slightly adjusting the cavity thickness during MBE growth. Adapted with permission from Geels *et al.*, *Proceedings of Optical Fiber Communication Conference*, Paper WB3, San Jose, Feb. 2, 1992 (OSA, Washington, DC, 1992). Copyright 1992, OSA (ripple due to imperfect AR coating). (b) Currents for various powers out for an improved gain-offset VCSEL with top and bottom AlAs-GaAs top and bottom DBRs having 18 and 17.5 periods, respectively, as well as with high-barrier $\text{Al}_{0.5}\text{Ga}_{0.5}\text{As}$ surrounding three $\text{In}_{0.185}\text{Ga}_{0.815}\text{As}$ QWs. The PL emission was at 972 nm, while the cavity mode was at 997 nm at 25 °C, yielding a 25 nm gain offset in this case. Adapted with permission from Young *et al.*, *IEEE Photonics Technol. Lett.* **5**, 129 (1993). Copyright 1993, IEEE.

the resonant wavelength is selected at a point where the absorption is low, the F-P cavity is imbalanced, and the reflection is high at zero bias. Then, as a bias is applied the absorption increases to the point where the cavity is balanced for zero reflection.

These reflection modulators are also capable of very high-speed modulation if designed and fabricated appropriately, because of their inherently low capacitance. To demonstrate this, ASFP devices were grown on semi-insulating substrates with mm-wave probe pads connecting to *intra-cavity* *p* and *n* contact layers grown immediately above and below the MQW active region. The wafers were then processed so that the probe pads rested only on the semi-insulating substrate with short traces running to the contact layers with the *n*-layer grounded and the *p*-layer to the signal line. The devices were tested with a Ti-sapphire laser, a high-speed photodetector, and a millimeter wave network analyzer. The results, shown in Fig. 4, indicate a 3 dB optical bandwidth of nearly 40 GHz with incident optical powers up to 100 μW . With higher incident powers, carrier generation in the quantum wells reduced the bandwidth to a little less than 20 GHz.³²

III. RESULTS ON VCSELS

A. Early VCSEL highlights

As outlined in Sec. I above, our initial electrically pumped VCSELS were processed with planarizing polyimide layers around the VCSEL mesa for contacts and silicon nitride antireflecting (AR) coatings on the rear substrate surface for better optical emission. A schematic is shown in Fig. 5 along with the initial results for a 12 μm mesa.¹⁴ The threshold current density of 800 A/cm² was the lowest reported for a VCSEL at the time.

As illustrated in Fig. 6, within a year (1991), the VCSEL effort had progressed to where CW output powers were over 1 mW with threshold currents less than 1 mA on small devices, and CW powers on larger devices exceeded 12 mW with pulsed outputs exceeding 100 mW¹⁵ (not shown). Fewer mirror periods

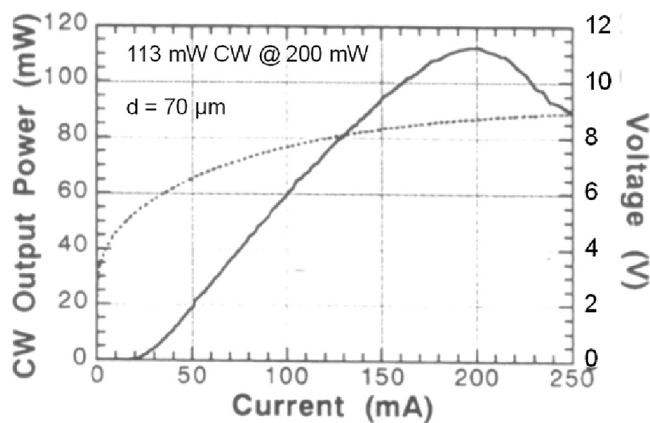


FIG. 8. CW output power and terminal voltage vs current for a 70 μm diameter device from the same material as in Fig. 7(b) mounted on a gold-plated diamond heat sink with indium solder. The diamond was mounted to a brass submount that rested on a thermo-electric cooler. VCSEL thinned to $\sim 100 \mu\text{m}$; diamond $\sim 250 \mu\text{m}$ thick; brass heat sink temperature was 20 °C. Adapted with permission from Peters *et al.*, *Electron. Lett.* **29**, 200 (1993). Copyright 1993, IEE.

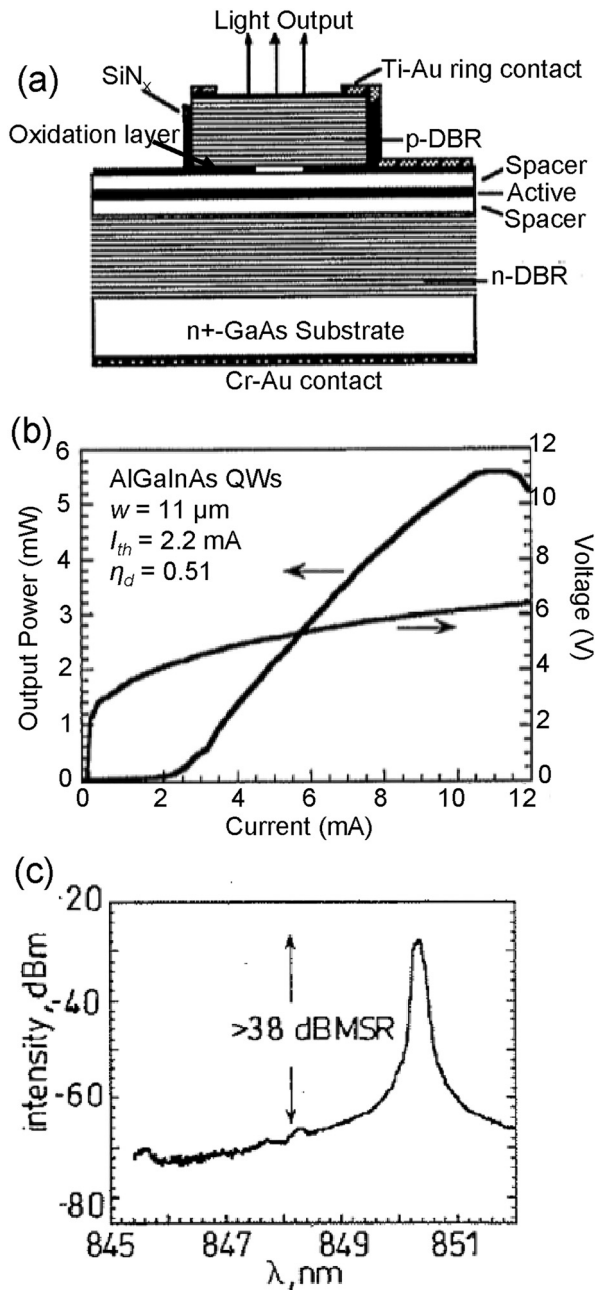


FIG. 9. Initial strained-layer, top-emitting, AlGaInAs QW VCSEL emitting at ~ 850 nm. (a) Bottom n-DBR had 25.5 periods of AlAs-Al_{0.1}Ga_{0.9}As and top p-DBR had 19 periods of Al_{0.9}Ga_{0.1}As—Al_{0.1}Ga_{0.9}As with graded interfaces. The active MQW used three 8 nm Al_{0.12}Ga_{0.66}In_{0.22}As wells with 50 nm Al_{0.2}Ga_{0.8}As barriers surrounded by 50 nm Al_{0.3}Ga_{0.7}As carrier confinement barriers and Al_{0.5}Ga_{0.5}As layers on each side to complete the one-wavelength cavity. (b) Output power and voltage vs applied current with inset spectrum at twice threshold. (c) Spectrum taken well above threshold. Adapted with permission from Ko *et al.*, *IEEE LEOS Annual Meeting*, Paper TuDD3, Boston, Nov. 19, 1996 (IEEE, Washington, DC, 1996). Copyright 1996, IEEE.

with lower doping were used, and three strained active quantum wells were employed.

In another few months, the concept of “gain offset” was introduced to improve the high temperature performance as shown in Fig. 7. This enabled VCSELs to operate to higher temperatures,¹⁶ but importantly, it also provided for nearly temperature independent

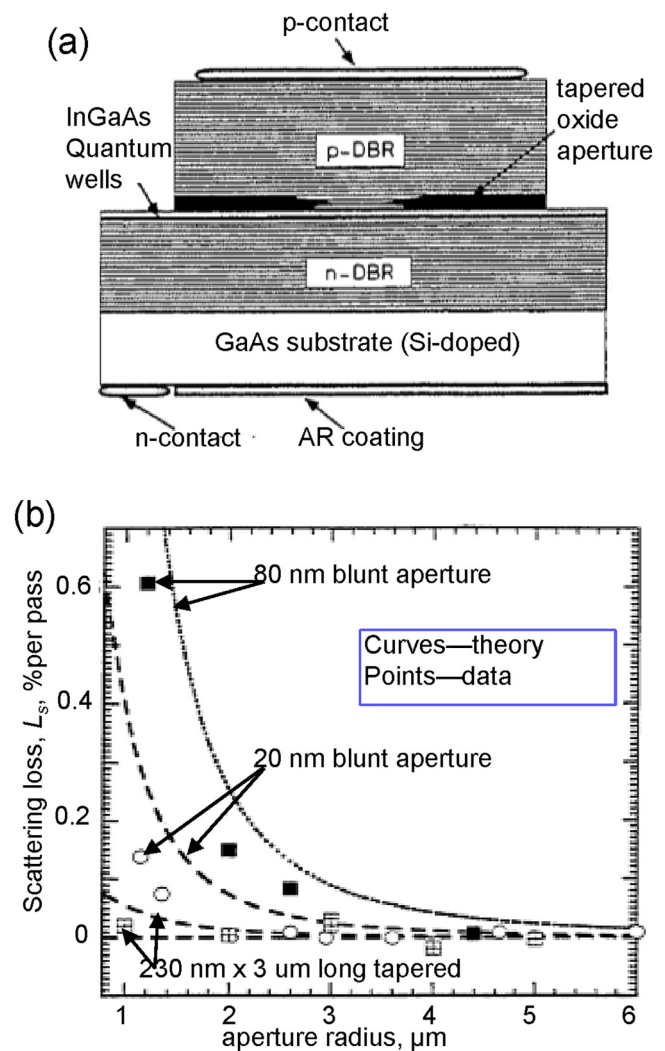


FIG. 10. Theoretical and experimental single pass optical losses in VCSELs with various oxide apertures. [Lowest theoretical dashed curve is for ideal parabolic taper to center of VCSEL—no data provided.] Bottom n-DBR has 18 AlAs-GaAs mirror periods; top p-DBR has 29.5 Al_{0.67}Ga_{0.33}As—GaAs periods with interfaces parabolically graded over 22 nm and step doped. Active has three 8 nm In_{0.18}Ga_{0.82}As with 8 nm GaAs barriers. The oxide apertures are above the active before the first mirror layer. Apertures are formed by oxidation of AlAs layers, placed at the standing wave null, next to Al_{0.9}Ga_{0.1}As. Oxidation is performed at 450 °C in water-saturated N₂. Adapted with permission from Hegblom *et al.*, *IEEE J. Sel. Top. Quantum Electron.* **3**, 379 (1997). Copyright 1997, IEEE.

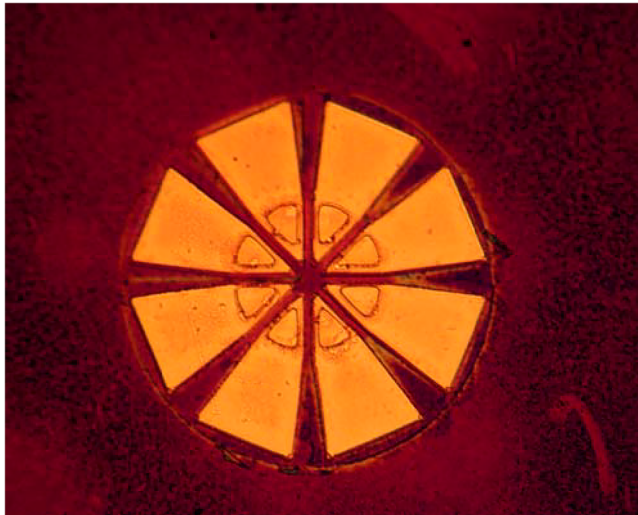


FIG. 11. Microphoto of an 8-wavelength photonic-integrated-emitter (PIE) array. CWDM wavelength spans of ~ 33 nm with element powers of ~ 2 – 7 mW were measured @ 15 mA/element (Ref. 23). Modulation speeds of >3 GHz with low crosstalk were also observed with improved electrode patterns. More information is found in Ref. 23.

operation at moderate temperatures.^{17,18} This can be accomplished because the gain maximum moves toward longer wavelengths about $4\times$ faster (3.3 nm/ 10°C) than does the cavity mode (0.8 nm/ 10°C); so if the mode is placed at a longer wavelength than the gain maximum at 20°C , then as the device is heated, the gain maximum moves toward the mode, eventually overtaking it, thereby compensating for the normal reduction in output power with increasing temperatures until it moves past. In part (a), we note that the threshold currents are nearly constant for temperatures from 25 to 45.5°C , and that the device operates with useful outputs to over 100°C . In part (b), it is directly shown that the threshold current and the current for some power out does not vary much over a wide temperature range.

Figure 8 illustrates what can be achieved with the same design described and characterized in Fig. 7(b), if the larger chips are mounted to a good heat sink—in this case with a diamond heat spreader. As can be seen, this enables a CW output power of about 113 mW with a room temperature heat sink, again another milestone at the time.¹⁹

Although strained InGaAs QWs with AlAs-GaAs DBRs proved to give the best VCSEL performance and reliability, the industry adopted an 850 nm wavelength standard due mainly to the existence of fiber that was optimized for this wavelength in the 1990s. Thus, many researchers focused their efforts on GaAs QWs with AlAs-AlGaAs DBRs, which provided VCSELs that emitted at 850 nm, but with reduced performance relative to the strained InGaAs QWs that emitted at ~ 980 nm. Therefore, realizing the many advantages of strain, we developed a strained-layer QW technology that added Al to our InGaAs materials to pull the wavelength down to 850 nm.

Figure 9 shows the first VCSEL results published with strained AlGaInAs QWs.²⁰ This followed work on edge-emitters to perfect the material.³³ These results compared very well to the state-of-the-art for 850 nm VCSELs of the time (1996).³⁴

For these results, the n^+ GaAs substrates were misoriented 2° toward $\langle 111 \rangle$ to reduce O_2 incorporation, and after growth the wafers were annealed by RTA for 10 s at 900°C .

With oxide or etched apertures, the current was constricted to a certain diameter above the active region, and it had been observed that lateral optical diffraction and scattering loss was somewhat limited because of the first-order lensing or waveguiding effect it provided.³⁵ However, a blunt aperture was far from a perfect lens (parabolic index variation) that was known to be needed from prior laser theory. Measurements had shown that optical loss, not due to free-carrier absorption, remained a major limitation on smaller devices. Therefore, we proposed to make this intracavity aperture into a better lens to reduce optical loss.²¹

Figure 10 gives the results of some modeling and data that indicates the potential of using tapered apertures compared to blunt apertures from VCSELs that were fabricated with oxide apertures. The theory uses an iterative mode recirculation algorithm to both find the mode and the round-trip loss.²² Not surprisingly, the improvement is especially important for smaller radius devices, where diffraction and aperture scattering loss would be particularly large. It is interesting to note that the measured data show more improvement than predicted from the modeling in the case of “blunt” apertures. This is probably due to the fact that there is also some significant tapering on the “blunt” apertures because of the manner in which they are constructed. That is, all of these apertures, and most in the literature, are formed from a layer of high Al content AlGaAs next to a modest Al content AlGaAs.

Because of the layer index requirements in the VCSEL, the Al content in both layers is generally quite high, usually pure AlAs or very high Al-fraction AlGaAs for the high Al layer and close to $\sim 90\%$ for the adjacent lower Al-fraction layer. Thus, as the high Al content layer oxidizes laterally, the lower Al content layer begins to oxidize vertically from the already oxidized layer. For example, if the lower Al content layer oxidizes at only 5% of the rate of the higher Al-content layer (the approximate ratio for 90% compared to $100\%\text{Al}$), we can see that it will oxidize vertically 100 nm at the edge of the sample for every 2000 nm the high Al-content layer oxidizes laterally, and it tapers linearly to the end of this high Al-content layer—so if we began with a 20 nm high Al content layer thickness, after 2000 nm of lateral oxidation, we will have a oxide taper from 20 to 120 nm in thickness over $2\ \mu\text{m}$. This is a significant taper!

A number of novel geometries were explored during the 1990s to respond to the expanding demand for data bandwidth and VCSEL performance needed for Datacom. Figure 11 shows a multiwavelength VCSEL array with eight different wavelength emitters all integrated within a $60\ \mu\text{m}$ diameter, so that eight data channels could be simultaneously launched into a $60\ \mu\text{m}$ core multimode fiber simply by butt-coupling this VCSEL to it.²³ Corresponding resonant-cavity detector arrays, analogous to the asymmetric resonant-cavity modulators in Sec. II above were also investigated.³⁶ (Note that each wavelength channel experiences ~ 9 dB inherent loss in this scheme.)

In order to make such devices, the MBE growth of the VCSELs was interrupted following growth of the active region and

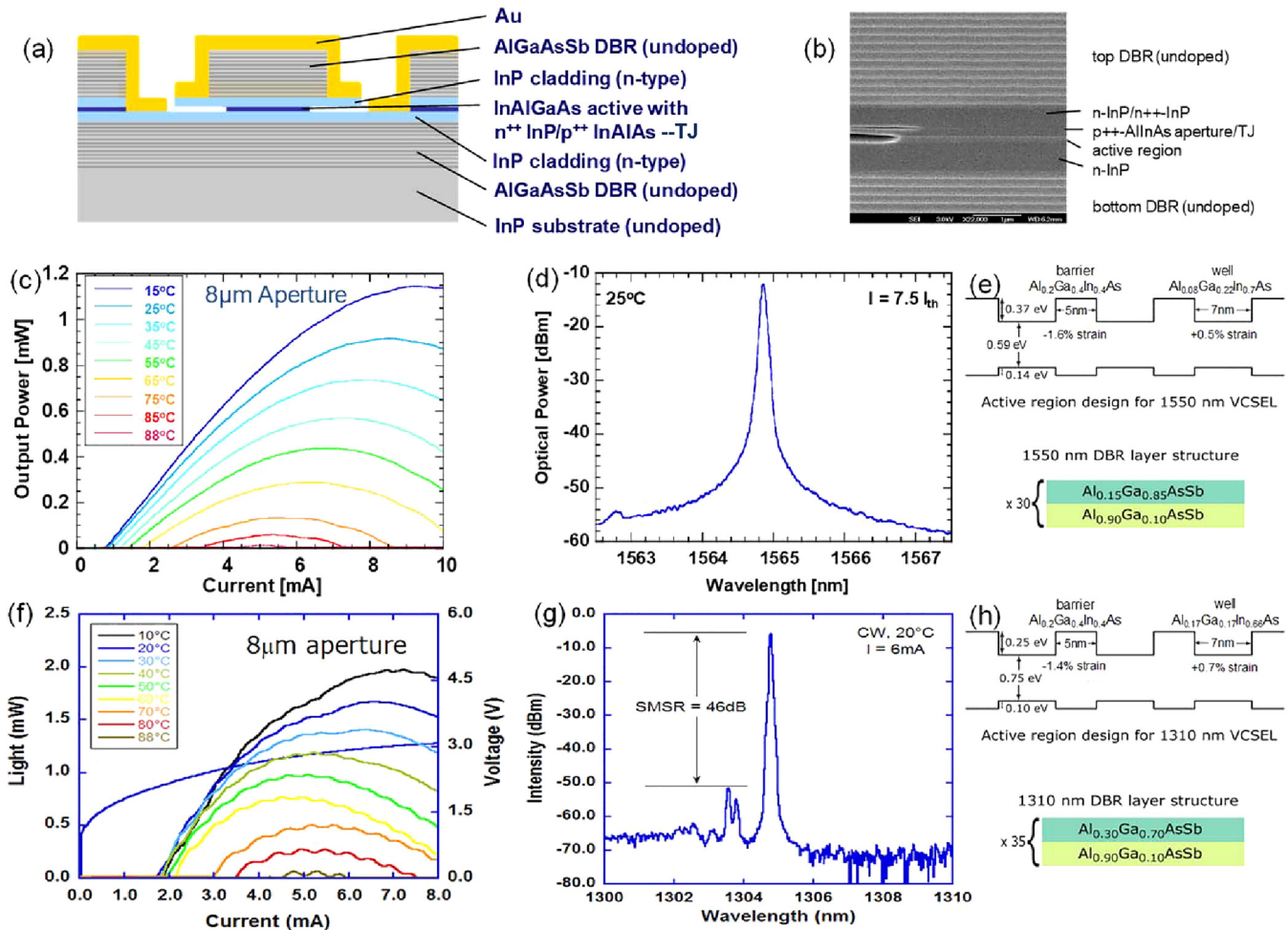


FIG. 12. InP-based 1310 and 1550 nm all-epitaxially grown VCSELs by MBE. (a) Schematic showing layers, mesa etching, and underetching following oxidation; (b) SEM cross section showing separate oxidation of AlInAs tunnel junction (TJ) layer and active region; (c) power-out vs current-in for a range of temperatures up to 88 °C for the VCSEL characterized by the spectrum in (d) (Ref. 24) that peaks at ~1565 nm at 25 °C; (e) active MQW and DBR mirror designs for (c) and (d); (f) power-out vs current-in for a range of temperatures up to 88 °C for the device characterized by the spectrum in (g) (Ref. 25) that peaks at 1305 nm at 20 °C; (h) active MQW and DBR mirror designs for (f) and (g). More information is found in Refs. 24 and 25.

first four top AlAs-GaAs mirror periods. The fourth GaAs mirror layer was grown 0.91λ thick instead of 0.25λ thick measured in the medium. Then, to get the eight different effective cavity lengths, this layer was successively patterned and very accurately etched using a three-level binary-coded anodic etching process over the VCSEL areas. Next, the wafer was reinserted into the MBE and the rest of the top mirror layers completed. Finally, the VCSEL array elements were completed in parallel in a single process sequence as used for other oxide-apertured VCSELs.

B. More recent VCSEL highlights

At the turn of the 21st century, it seemed clear that in-plane cavity, edge-emitters would dominate the long-haul communications

and high-power sensor marketplace. It also seemed clear that such high-performance components would tend to be high-cost and the market volume low. However, there still appeared to be the higher-volume short-to-medium-haul Datacom market, the longer-distance data-center market, and the lower-power sensor market, which all used single-mode fibers, that might support an effort on 1310 and 1550 nm VCSELs. Although there had been some successful work with wafer-bonded³⁷ and dielectric-mirror VCSELs³⁸ that operated in this range, we believed an all-epitaxial device that could mimic our successes with the shorter wavelength work would be worth exploring.

Thus, we designed and began to grow all-epitaxial AlGaAsSb/AlGaInAs/InP VCSELs by MBE. Given existing experience at UCSB with growing the antimonides in our system-B,³⁹ the quaternaries

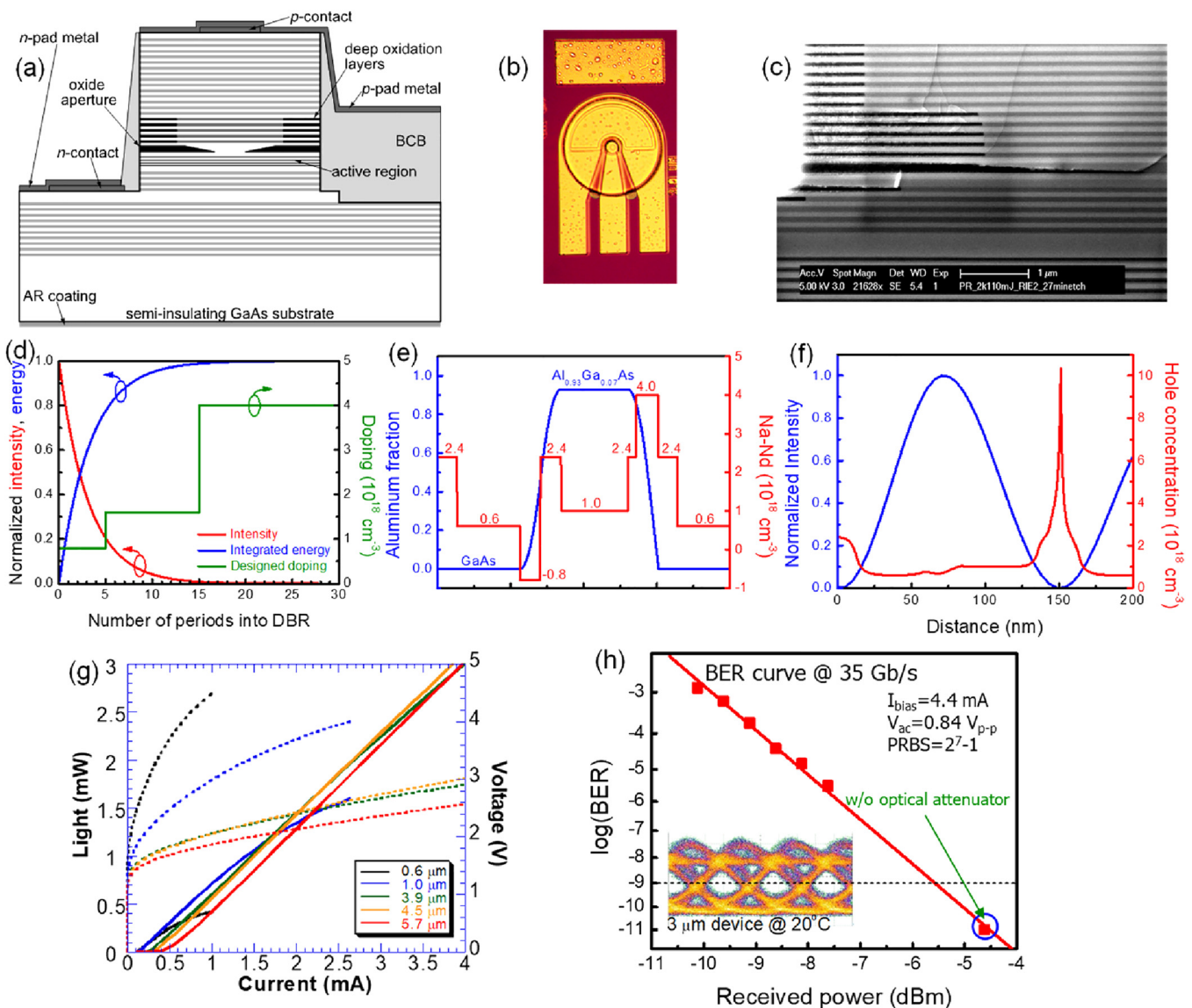


FIG. 13. (a) Schematic of high-speed, high-efficiency VCSEL @ 980 nm. (b) Microphoto of top metallization. (c) SEM cross section showing depths of wet oxidation in mirrors, deep oxidation layers and tapered aperture; top p-DBR mirror has 25 periods of $\text{Al}_{0.85}\text{Ga}_{0.15}\text{As-GaAs}$ on top of five periods of $\text{Al}_{0.93}\text{Ga}_{0.07}\text{As-GaAs}$ for deep oxidation; aperture layer is $\lambda/2$ thick with $\text{Al}_{0.93}\text{Ga}_{0.07}\text{As}$ on top of 20 nm of AlAs; active has high-barrier $\text{Al}_{0.5}\text{Ga}_{0.5}\text{As}$ layers surrounding three 8 nm $\text{In}_{0.185}\text{Ga}_{0.815}\text{As}$ QWs with 8 nm GaAs barriers; the bottom DBR mirror first has 4 periods of n-doped $\text{Al}_{0.9}\text{Ga}_{0.1}\text{As-GaAs}$, then a $5/4\text{-}\lambda$ n^+ contact layer, and finally 14 periods of undoped AlAs-GaAs. (d) Designed doping, optical intensity, and integrated energy vs number of periods into the top p-DBR. (e) Designed doping over one p-mirror period. (f) Hole concentration and optical mode intensity over one p-mirror period. (g) Optical output and terminal voltage vs current in for five different device diameters. (h) Log bit-error-rate vs received power and inset eye-diagram @ 35 Gb/s for a $3\text{-}\mu\text{m}$ device. As described in Ref. 29.

were not a major challenge, especially with Prof. Gossard's contributions to digital superlattices.⁴⁰ Actually, growing the InP on top of many micrometers of the quaternaries was a bit more difficult, given that InP cannot adjust its lattice constant very much.

Figure 12 gives results for both 1310 (actually 1305 nm)²⁵ and 1550 (actually 1565 nm)²⁴ AlGaAsSb-DBR/AlGaInAs-Active/InP

VCSELs. They have a number of that features enable high-yield, high-performance VCSELs with potential low-manufacturing costs.

Key features include (1) high-index-of-refraction differences within the Sb-based DBR mirrors, which give nearly the same index contrast as for the AlGaAs system @ 850 nm; (2) embedded $n^+\text{InP}/p^+\text{AlInAs}$ tunnel junctions just above the MQW active

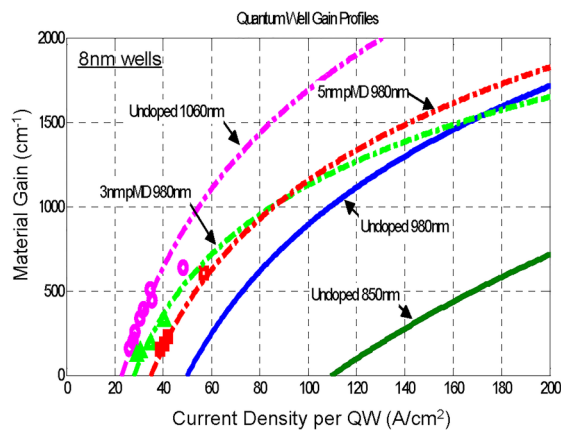


FIG. 14. Material gain of 8 nm quantum wells of GaAs/AlGaAs (green-solid) and strained InGaAs/GaAs; gain only measured at lower quantum state with little population in upper state. p-type modulation doping (pMD) of the 8 nm GaAs barriers between and beside the InGaAs 980 nm wells by doping at 2×10^{18} over either 3 or 5 nm in barrier center. Adapted with permission from Coldren *et al.*, *Proceedings of IEEE Photonics Society Summer Topical Meeting, Paper TuD2.1*, Playa Del Carmen, Mexico, July 19, 2010 (IEEE, Washington, DC, 2010). Copyright 2010, IEEE.

region that enables two binary n-type InP cladding/contact layers for both low electrical and thermal resistance to the active area as well as undoped mirrors; (3) built-in aperturing layers with the AlInAs tunnel junction and high-Al fraction AlGaInAs active barriers for low optical loss and little current spreading; and (4) a single all-epitaxial growth step to avoid complex multistep bonding or critical postdeposition processes for mirrors.

Meanwhile, high-volume shorter distance links (≤ 30 m) with multimode fibers (or even printed waveguides on circuit boards) for Datacom and interconnects within supercomputers or switching racks called for low-cost, high-speed, high-efficiency shorter wavelength VCSELs. Thus, an effort was established to make the highest-speed, highest-efficiency VCSEL using all of the tricks developed previously as well as a new CB_4 doping system for low-diffusion high-carbon doping in our newest Gen-III system.

Figure 13 summarizes some of the design aspects and results for these new VCSELs.^{28–30} As can be seen, some sophisticated bandgap engineering and modulation doping was incorporated to reduce the p-mirror resistance without increasing optical loss. Also, intracavity deep-oxidation layers were added by increasing the aluminum fraction in the first five mirror layers from 85% to 93% to increase the lateral oxidation by about $3 \times$ and thereby reduce capacitance without decreasing the contact resistance. In addition,

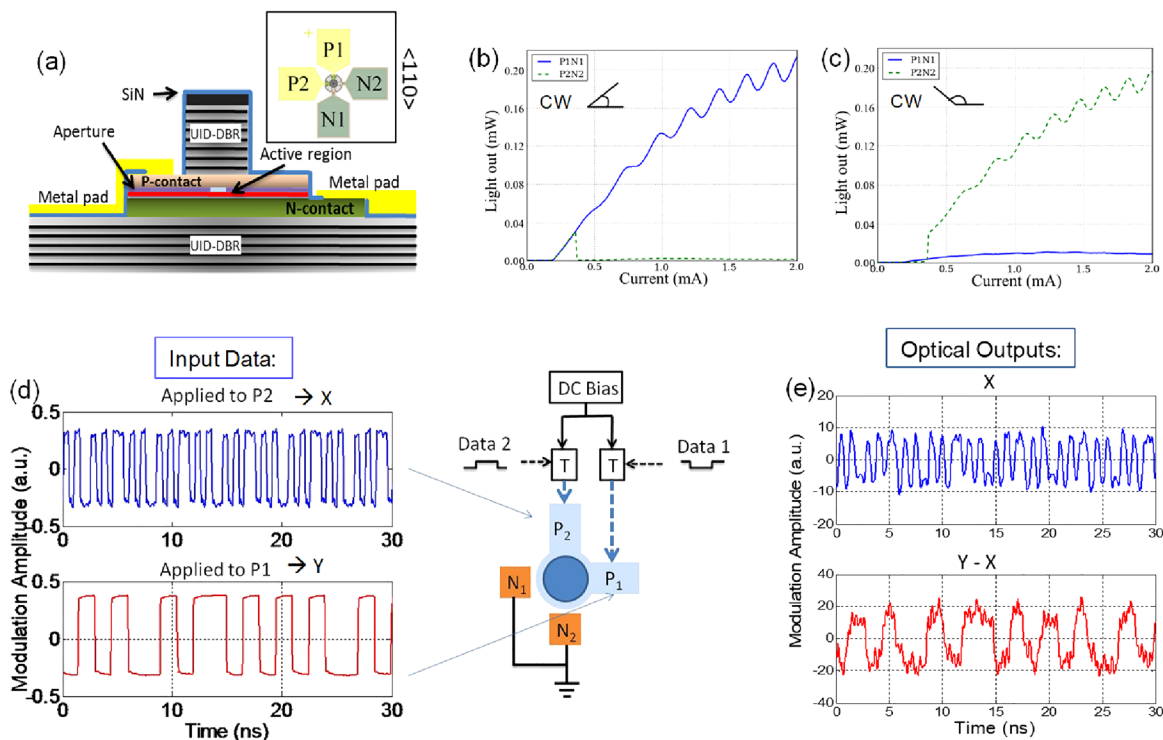


FIG. 15. Multiterminal polarization-modulated VCSEL. (a) Schematic cross section and top labeling of electrodes for the two channels; (b) light-out in two orthogonal polarizations vs current-in for current applied across P1-N1; (c) light-out in two orthogonal polarizations vs current-in for current applied across P2-N2; (d) data applied to two electrode pairs and schematic of experiment; (e) optical outputs: X is on polarization as in (c)—a replica of the signal to P2; however, the operation $Y-X$ is required to remove crosstalk from the orthogonal polarization as in (b) to obtain a replica of the signal to P1. (a)–(c) described in Ref. 26; (d) and (e) described in Ref. 27.

the tapered aperture was made somewhat blunter than the $3\mu\text{m}$ long design illustrated in Fig. 11 for a smaller optical mode by increasing the composition of the aluminum to 93% in the AlGaAs next to the ALAs that leads the oxidized aperture point. All of these features improve efficiency and modulation speed.

At the time of initial publication (2007), the data rate efficiency of 286 fJ/bit was a new record for a VCSEL,²⁸ and this record stood for four years.⁴¹ A few years later (2010), a similar device was used in a full link test at IBM, and the full-link value (without timing recovery) was 0.9 pJ/bit, also a new milestone.⁴²

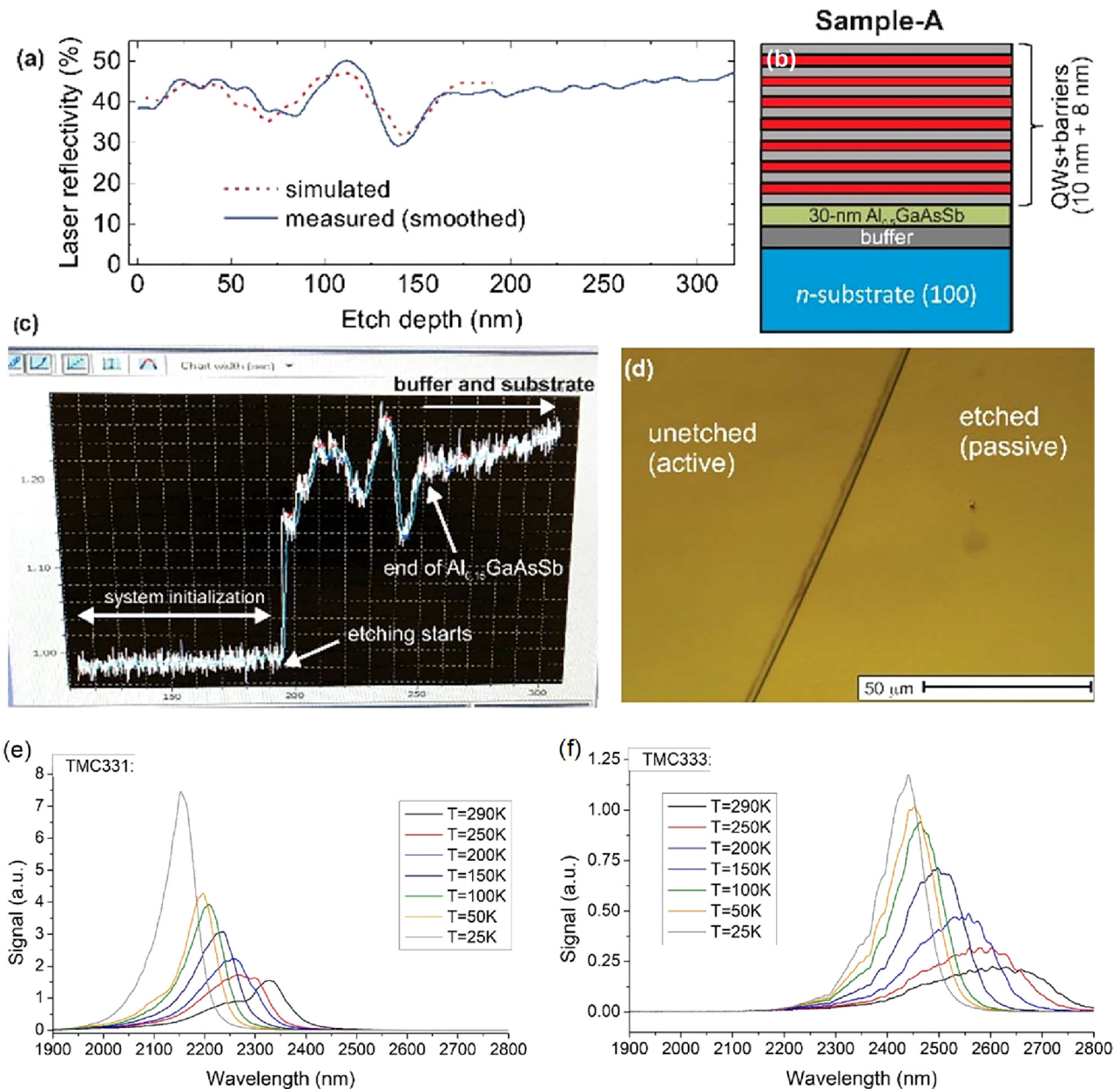


FIG. 16. Selective dry etching of MQW active from AlGaAsSb/GaSb and PL spectra. (a) Comparison of simulation and experimental laser reflectivity monitor data for Cl_2/N_2 reactive-ion-etching of the MQW layers; (b) schematic of grown samples containing seven MQW periods with 10 nm $\text{In}_{0.53}\text{Ga}_{0.47}\text{As}_y\text{Sb}_{1-y}$ wells and 8 nm GaSb barriers with a final 350 nm layer of GaSb followed by an $\text{Al}_{0.5}\text{Ga}_{0.5}\text{AsSb}$ lower cladding/end-etch layer; (c) actual laser-monitor data (note larger time window); (d) microphoto of wafer surface comparing etched and unetched regions; (e) active-region PL spectra at various temperatures for the test sample; and (f) PL spectra for a sample with a higher In fraction in the QWs. [(a)–(d): Adapted with permission from Arafin *et al.*, *Opt. Mater. Express* **9**, 1786 (2019). Copyright 2019, OSA; (e)–(f): unpublished].

The data-rate-efficiency record of ~ 160 fJ/bit set by Furukawa in 2011⁴¹ was short lived, since this was then one of the recognized figures-of-merit to satisfy the increasing demand for improved data-link efficiency both in data centers and super computers. Accordingly, VCSELs with efficiencies of 81 fJ/bit⁴³ and then 69 fJ/bit⁴⁴ soon followed later in 2011 and 2012, respectively, from the TU-Berlin/VI-Systems team.

The Furukawa result benefitted from the use of a 1060 nm highly strained InGaAs MQW active.⁴¹ In fact, as summarized in Fig. 14, we had done an earlier MBE study of highly strained and modulation-doped quantum-well gain regions to identify candidates for improved optical modulation speed and efficiency,⁴⁵ which clearly pointed out that the most highly strained InGaAs quantum wells at 1060 nm would require about half the current for a given gain as well as provide significant increases in the differential gain. In a laser, the maximum modulation frequency is proportional to the square root of the differential gain, and the threshold current would almost be halved in switching from 980 to 1060 nm.⁴⁶ This explains the Furukawa result.

Another method of increasing bit rate on a single optical beam is the use both polarizations. In order to avoid polarization multiplexing hardware and to do this in a single device, switching between VCSEL polarizations as well as the modulation of the individual polarizations was explored. As others had investigated,⁴⁷ we utilized the concept of asymmetric current injection to attempt to distort the carrier k-vector distribution in the quantum-well gain regions, and thus, to introduce some gain anisotropy and thereby favor a particular lasing polarization.

Figure 15 summarizes some of the design concepts and results.^{26,27} As shown in part (a), four electrodes are used with pairs of p- and n-contacts opposite each other to intracavity contacts together with some degree of electrical isolation to implement some degree of lateral current flow in the active region. As the data shows, the CW optical polarization can be switched by switching currents between the two pairs of contacts, but more importantly, two different data streams can be simultaneously applied to the two pairs of contacts, and then be remotely deciphered. This experiment suggested that up to 16 Gb/s might be transmitted by such a multiterminal VCSEL, even though it was parasitically bandwidth limited to a single-channel bit rate of 8 Gb/s in this case.²⁷

The most recent effort that my group led was in direct collaboration with Prof. Palmstrøm to fabricate short-wave infrared (SWIR) lasers based on GaSb, initially in the 2–3 μm wavelength range. InGaAsSb/AlGaAsSb/GaSb MQW gain regions and AlAsSb/GaSb DBR mirrors were considered for VCSELs and this same MQW gain region with AlGaAsSb cladding regions were considered for edge-emitters. Figure 16 summarizes some results of growth and processing.³¹ The Gen-III system was again employed. Smooth layers with good photoluminescence were grown and the necessary processing technology for lasers was also developed.

IV. SUMMARY AND CONCLUSIONS

In this paper, I have reviewed a segment of the work that Prof. Arthur Gossard has enabled while at UC-Santa Barbara—some highlights of work on vertical-cavity modulators and lasers, all-epitaxially grown by MBE. Although Art was not always a coauthor on the

published papers, his contributions in guiding the graduate students and postdocs as well as in keeping the MBE lab running extremely well were always key to the success of the projects.

Although JVST guidelines mention that one should avoid claims that results are the *first* or have the *best* characteristics in some important recognized aspect at the time of reporting, I have endeavored to limit the selection of highlighted results to only those that must be described in this manner for accuracy. My goal is to point out that Prof. Gossard has enabled some highly impactful work that has had and continues to have a major influence in our scientific and business communities. For example, VCSELs have penetrated many markets today, and the volume of sales is measured in the tens of millions of devices per month. Many of the designs developed and demonstrated in Art's MBE lab are incorporated within these devices, and moreover, many of the student coauthors referenced in this paper are either in leadership positions or are directly producing such products within the major manufacturers today. Many others who worked in Art's MBE lab can also be added to that group.

Art continues to be involved in a number of important MBE projects as outlined in other papers in this issue.

ACKNOWLEDGMENTS

Although this paper focuses on the contributions of Gossard, I also want to acknowledge the extremely important contributions of John English in training and mentoring all of the graduate students involved with MBE growth as well as his many scientific contributions to the research reported. I want to acknowledge funding support from AFOSR for the modulator work, and DARPA-MTO via the Optoelectronics Technology Center for supporting much of the VCSEL work. Funding from and collaboration with Honeywell, Raytheon, IBM, Hewlett-Packard, and Rockwell Scientific are gratefully acknowledged as well.

DATA AVAILABILITY

Data sharing is not applicable to this article as no new data were created or analyzed in this study.

REFERENCES

- ¹G. D. Boyd, D. A. B. Miller, D. S. Chemla, S. L. McCall, A. C. Gossard, and J. H. English, *Appl. Phys. Lett.* **50**, 1119 (1987).
- ²D. A. B. Miller, *Opt. Eng.* **26**, 368 (1987).
- ³R. J. Simes, R. H. Yan, R. Geels, L. A. Coldren, J. H. English, and A. C. Gossard, *CLEO'88*, Paper TuE2, Anaheim, Apr. 26, 1988 (OSA, Washington, DC, 1988).
- ⁴R. J. Simes, R. H. Yan, R. Geels, L. A. Coldren, J. H. English, A. C. Gossard, and D. G. Lishan, *Appl. Phys. Lett.* **53**, 637 (1988).
- ⁵R. H. Yan, R. J. Simes, and L. A. Coldren, *IEEE Photonics Technol. Lett.* **1**, 273 (1989).
- ⁶R. H. Yan, R. J. Simes, L. A. Coldren, and A. C. Gossard, *Appl. Phys. Lett.* **56**, 1626 (1990).
- ⁷K. K. Law, M. Whitehead, J. L. Merz, and L. A. Coldren, *Electron. Lett.* **27**, 1863 (1991).
- ⁸D. A. B. Miller, D. S. Chemla, T. C. Damen, A. C. Gossard, W. Wiegmann, T. H. Wood, and C. A. Burrus, *Phys. Rev. Lett.* **53**, 2173 (1984).

- ⁹R. Geels, R. H. Yan, J. W. Scott, S. W. Corzine, R. J. Simes, and L. A. Coldren, *Proceedings of Conference on Lasers and Electro-Optics*, Paper WM1, Anaheim, Apr. 27, 1988 (OSA, Washington, DC, 1988).
- ¹⁰S. W. Corzine, R. Geels, J. W. Scott, and L. A. Coldren, *Proceedings of IEEE Lasers & Electro-Optics Society Annual Meeting*, Paper OE1.2, Santa Clara, Nov. 2, 1988 (IEEE, Washington, DC, 1988).
- ¹¹L. A. Coldren, J. W. Scott, and R. H. Yan, U.S. patent 4,873,696 (10 October 1989).
- ¹²S. W. Corzine, R. S. Geels, J. W. Scott, R. H. Yan, and L. A. Coldren, *IEEE J. Quantum Electron.* **25**, 1513 (1989).
- ¹³J. L. Jewell, A. Scherer, S. L. McCall, Y. H. Lee, S. J. Walker, J. P. Harbison, and L. T. Florez, *Electron. Lett.* **25**, 1123 (1989).
- ¹⁴R. S. Geels, S. W. Corzine, J. W. Scott, D. B. Young, and L. A. Coldren, *Proceedings of Optical Fiber Communication Conference*, Paper PD31-1, San Francisco, Jan. 24, 1990 (OSA, Washington, DC, 1990).
- ¹⁵R. S. Geels and L. A. Coldren, *Electron. Lett.* **27**, 1984 (1991).
- ¹⁶R. S. Geels, S. W. Corzine, B. Thibeault, and L. A. Coldren, *Proceedings of Optical Fiber Communication Conference*, Paper WB3, San Jose, Feb. 2, 1992 X473 (OSA, Washington, DC, 1992).
- ¹⁷S. W. Corzine, J. W. Scott, R. S. Geels, D. B. Young, B. Thibeault, M. Peters, and L. A. Coldren, *Proceedings of IEEE LEOS Summer Topical Meeting on Optics*, Paper ThB5, Santa Barbara, Aug. 7, 1992 (IEEE, Washington, DC).
- ¹⁸D. B. Young, J. W. Scott, F. H. Peters, B. J. Thibeault, S. W. Corzine, M. G. Peters, S. L. Lee, and L. A. Coldren, *IEEE Photonics Technol. Lett.* **5**, 129 (1993).
- ¹⁹F. H. Peters, M. G. Peters, D. B. Young, J. W. Scott, B. J. Thibeault, S. W. Corzine, and L. A. Coldren, *Electron. Lett.* **29**, 200 (1993).
- ²⁰J. Ko, B. J. Thibeault, Y. Akulova, E. R. Hegblom, D. B. Young, and L. A. Coldren, *IEEE LEOS Annual Meeting*, Paper TuDD3, Boston, Nov. 19, 1996 (IEEE, Washington, DC, 1996).
- ²¹L. A. Coldren, B. J. Thibeault, E. R. Hegblom, G. B. Thompson, and J. W. Scott, *Appl. Phys. Lett.* **68**, 313 (1996).
- ²²E. R. Hegblom, D. I. Babic, B. J. Thibeault, and L. A. Coldren, *IEEE J. Sel. Top. Quantum Electron.* **3**, 379 (1997).
- ²³S. Y. Hu, J. Ko, and L. A. Coldren, *IEEE Photonics Technol. Lett.* **10**, 766 (1998).
- ²⁴S. Nakagawa, E. Hall, G. Almuneau, J. K. Kim, D. A. Buell, H. Kroemer, and L. A. Coldren, *Appl. Phys. Lett.* **78**, 1337 (2001).
- ²⁵D. Feezell, L. A. Johansson, D. A. Buell, and L. A. Coldren, *IEEE Photonics Technol. Lett.* **17**, 2253 (2005).
- ²⁶Y. Zheng, C. H. Lin, and L. A. Coldren, *Electron. Lett.* **46**, 1619 (2010).
- ²⁷A. V. Barve, A. Mehta, A. Husain, and L. A. Coldren, *IEEE Optical Interconnects Conference*, Paper TuC5, San Diego, May 5, 2014 (IEEE, Washington, DC).
- ²⁸Y. C. Chang, C. S. Wang, and L. A. Coldren, *Electron. Lett.* **43**, 1022 (2007).
- ²⁹Y.-C. Chang and L. A. Coldren, *IEEE J. Spec. Top. Quantum Electron.* **15**, 704 (2009).
- ³⁰Y. C. Chang and L. A. Coldren, U.S. patent 7,916,768 B2 (29 March 2011).
- ³¹S. Arafin, A. P. McFadden, B. Paul, S. M. N. Hasan, J. A. Gupta, C. J. Palmström, and L. A. Coldren, *Opt. Mater. Express* **9**, 1786 (2019).
- ³²C. C. Barron, C. J. Mahon, B. J. Thibeault, G. Wang, J. R. Karin, L. A. Coldren, and J. E. Bowers, *Device Research Conference*, Paper VIB-9, Santa Barbara, Jun. 23, 1993 (IEEE, Washington, DC, 1993); *ibid.* *IEEE LEOS'93*, Paper SP1.2, San Jose, Nov. 15, 1993 (IEEE, Washington, DC, 1993).
- ³³J. Ko, M. J. Mondry, D. B. Young, S. Y. Hu, L. A. Coldren, and A. C. Gossard, *Electron. Lett.* **32**, 351 (1996).
- ³⁴J. K. Guenter, R. A. Hawthorne, D. N. Granville, M. K. Hibbs-Brenner, and R. A. Morgan, *Proc. SPIE* **2683**, 102 (1996).
- ³⁵K. L. Lear, K. D. Choquette, R. P. Schneider, and S. P. Kilcoyne, *Appl. Phys. Lett.* **66**, 2616 (1995).
- ³⁶O. Sjolund, D. A. Louderback, E. R. Hegblom, J. Ko, and L. A. Coldren, *IEEE J. Quantum Electron.* **35**, 1015 (1999).
- ³⁷N. M. Margalit *et al.*, *IEEE J. Sel. Top. Quantum Electron.* **3**, 359 (1997).
- ³⁸Y. Qian, Z. H. Zhu, Y. H. Lo, D. L. Huffaker, D. G. Deppe, H. Q. Hou, B. E. Hammons, W. Lin, and Y. K. Tu, *IEEE Photonics Technol. Lett.* **9**, 866 (1997).
- ³⁹G. Tuttle, H. Kroemer, and J. H. English, *J. Appl. Phys.* **67**, 3032 (1990).
- ⁴⁰M. Sundaram, A. Wixforth, R. S. Geels, A. C. Gossard, and J. H. English, *J. Vac. Sci. Technol. B* **9**, 1524 (1991).
- ⁴¹S. Imai *et al.*, *IEEE J. Sel. Top. Quantum Electron.* **17**, 1614 (2011).
- ⁴²S. Nakagawa, *Industrial Forum—Asia Conference on Photonics (ACP2011)*, Shanghai, China, Nov. 13, 2011 (OSA, Washington, DC, 2011).
- ⁴³P. Moser, W. Hofmann, P. Wolf, J. A. Lott, G. Larisch, A. Payusov, N. N. Ledentsov, and D. Bimberg, *Appl. Phys. Lett.* **98**, 231106 (2011).
- ⁴⁴P. Moser, J. A. Lott, P. Wolf, G. Larisch, A. Payusov, G. Fiol, N. N. Ledentsov, W. Hofmann, and D. Bimberg, *Proc. SPIE* **8276**, 82760J (2012).
- ⁴⁵L. A. Coldren, Y. C. Chang, Y. Zheng, and C. H. Lin, *Proceedings of IEEE Photonics Society Summer Topical Meeting*, Paper TuD2.1, Playa Del Carmen, Mexico, Jul. 19, 2010 (IEEE, Washington, DC, 2010).
- ⁴⁶L. A. Coldren, S. W. Corzine, and M. Mašanović, *Diode Lasers and Photonic Integrated Circuits*, 2nd ed. (Wiley, NY, 2012), Chap. 5.
- ⁴⁷L. M. Augustin, E. Smalbrugge, K. D. Choquette, F. Karouta, R. C. Stribos, G. Verschaffelt, E. J. Geluk, T. G. van de Roer, and H. Thienpont, *IEEE Photon. Technol. Lett.* **16**, 708 (2004).